BASIC RESEARCH

# Effect of Asymmetric Tension on Biomechanics and Metabolism of Vertebral Epiphyseal Plate in a Rodent Model of Scoliosis

Qian-yi Li, MD, Gui-bin Zhong, MD, Zu-de Liu, MD, Li-feng Lao, MD

*Department of Orthopaedic Surgery, Renji Hospital, School of Medicine, Shanghai Jiao Tong University, Shanghai, China*

**Objective:** To investigate the effect of asymmetric tension on idiopathic scoliosis (IS) and to understand its pathogenic mechanism.

**Methods:** The rodent model of scoliosis was established using Sprague–Dawley rats with left rib-tethering from $T_6$ to $T_{12}$, tail and shoulder amputation, and high-cage feeding. Vertebrae epiphyseal cartilage plates were harvested from the convex and concave sides. To analyze differences on the convex and concave sides, finite element analysis was carried out to determine the mechanical stress. Protein expression on epiphyseal cartilage was evaluated by western blot. Micro-CT was taken to evaluate the bone quality of vertebral on both sides.

**Results:** Scoliosis curves presented in X-ray radiographs of the rats. Finite element analysis was carried out on the axial and transverse tension of the spine. Stresses of the convex side were −170.14, −373.18, and −3832.32 MPa (X, Y, and Z axis, respectively), while the concave side showed stresses of 361.99, 605.55, and 3661.95 MPa. Collagen type II, collagen type X, Sox 9, RunX2, VEGF, and aggrecan were expressed significantly more on the convex side ($P < 0.05$). There was asymmetric expression of protein on the epiphyseal cartilage plate at molecular level. Compared with the convex side, the concave side had significantly lower value in the BV/TV and Tb.N, but higher value in the Tb.Sp ($P < 0.05$). There was asymmetry of bone quality in micro-architecture.

**Conclusions:** In this study, asymmetric tension contributed to asymmetry in protein expression and bone quality on vertebral epiphyseal plates, ultimately resulting in asymmetry of anatomy. In addition, asymmetry of anatomy aggravated asymmetric tension. It is the first study to show that there is an asymmetrical vicious circle in IS.

**Key words:** Asymmetric tension; Biomechanics; Epiphyseal plate; Metabolism; Scoliosis

## Introduction

The prevalence of idiopathic scoliosis (IS) in young people is 2%–4%[1]. It is a multi-factorial disease with unclear etiology, which is possibly attributed to genetic factors, growth abnormalities, hormonal and neuromuscular dysfunction. Surgical treatment of IS is associated with high risk, cost and postoperative recurrence; thus, it can result in a heavy economic and psychological burden to families and society.

Scoliosis has never been found in vertebrates other than humans[2]. A key reason that human vertebrates are different from others is that humans walk upright. The position of center-of-gravity is located above the pelvis in the human body. A number of relevant animal models have been created, including pinealectomy in a chicken model, an immature goat model, and a porcine early-onset model[3–5]. Among all such models, a bipedal rat model simulated human upright walking well.

The vertebral epiphyseal plate is a hyaline cartilage plate in the metaphysis. The growth of the human spine mainly relies on the upper and lower sides of the epiphyseal plate by continuous development and proliferation. The

**Address for correspondence** Li-feng Lao, MD, Department of Orthopaedic Surgery, Renji Hospital, School of Medicine, Shanghai Jiao Tong University, Shanghai, China 200127 Tel: 0086-013701899053; Fax: 0086-21-58394262; Email: laolifeng@gmail.com

**Disclosure:** This study was supported by the Shanghai Pujiang Program (No. 15PJD026), the National Natural Science Foundation of Youth Program (No. 81101394), the Medical-Engineering Joint Fund of Shanghai Jiao Tong University (No. YG2014MS51), and the Incubating Program for Clinical Research and Innovation of Renji Hospital (PYXJS16-006).
Received 11 August 2016; accepted 3 December 2016



Orthopaedic Surgery

orientation of collagen fibers in the growth plate and contiguous structures of a growing long bone were demonstrated by polarized light microscopy. Five major groups of collagen fibers were established: transphyseal (longitudinal), perichondrial–periosteal (longitudinal), epiphyseal (radial), perichondrial ring (circumferential), and metaphyseal bone (circumferential)[6]. These fiber groups are staggered to form a collagen fiber web. This structural basis determines the mechanical properties of the epiphyseal plate

The human body is asymmetrical. Kouwenhoven and other scholars analyzed CT images of normal spine segments and identified a rotation to the left in the high thoracic vertebrae, whereas there was a rotation to the right in lower segments[7]. Asymmetric tension in scoliosis is reflected in muscle hypertrophy of the concave side and muscle atrophy of the convex side[8]. In recent years, through anatomical studies of scoliosis patients, asymmetry has been found to arise from discs, which results in distortion of the epiphyseal cartilage[9]. Wolff's theories state that vertebral body shape change is the result of force, and force is the direct effect of the micro-structure of the vertebral epiphyseal plate, which changes before scoliosis[10]. Axial load (perpendicular to the main plane of the epiphyseal plate) can accelerate or reduce the osteogenesis of the epiphyseal plate. Furthermore, shear load can make the vertebrae tilt, intermittent torsion contributes to its rotation, and sustained load can change the viscoelastic properties of epiphyseal plate. The range of the load value and the time of its action are two important determinants of vertebral development. This view reflects our understanding of the complex biological and biomechanical multifactorial processes[11].

Scoliosis is a 3-D deformity, and mechanical imbalance is the key factor in the occurrence and development of scoliosis. At present, the research method applied to scoliosis is mainly retrospective analysis of clinical cases due to the lack of an effective scoliosis model. Research on the effect of asymmetric tension on the growth of scoliosis generally as well as from the perspective of biomechanics and molecular biology is still lacking.

In this study, we assume that there is a biomechanical or metabolic pathway through which asymmetric tension leaded to scoliosis. This study is the first to investigate the effect of asymmetric tension on IS, and follows three steps: (i) to investigate the feasibility of a rodent model of scoliosis; (ii) to demonstrate the differences in mechanical stress, protein expression, and bone quality on the convex and concave sides; and (iii) to explore the relationships among stress, protein expression, bone quality, and asymmetry of anatomy.

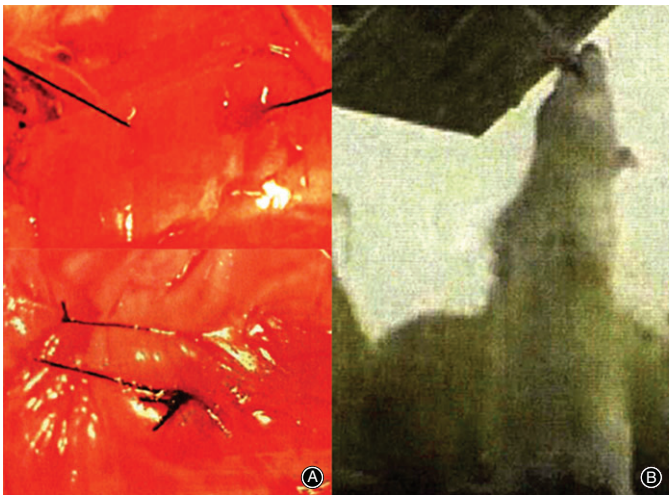


**Fig. 1** An operation was performed at 4 weeks after birth (A). Rats were fed in high cages (B).

## Methods

### *Animal Models*

Eight 4-week-old virgin female Sprague–Dawley rats (weight: 65–75 g) were housed in a laboratory at 22.2°C under a 12-h light and 12-h dark cycle and maintained on a Purina laboratory rodent chow diet (The second Military Medical University, Shanghai, China). An operation was performed at 4 weeks after birth, with: (i) left rib tethering procedure from $T_6$ to $T_{12}$ with a nonadsorbable No. 0 suture (Ethicon, Somerville, NJ, USA); (ii) tail amputation; (iii) shoulders amputation; and (iv) rats fed in high cages. Rats remained upright most of the time (Fig. 1). At the end of the 4-week treatment, an X-ray of the total spine was taken (Fig. 2). Rats with Cobb angle >10° were euthanized, and the apical vertebra of rats is $T_{11}$. This study was approved by the ethics committee of the hospital.

### *Finite Element Analysis*

#### *Development of Finite Element Model*

In a 17-mm sample holder in the cranial–caudal direction, the spine ($T_8$–$L_1$) was scanned using a high-resolution μCT system (μCT35, Scanco, MicroCT systems and Software, Brüttisellen, Zurich, Switzerland). After scanning, the 2-D image data was converted to 3-D images using Mimics 17 (Materialise's interactive medical image control system, Materialise, Belgium). The reconstructed images of one apical vertebra ($T_{11}$) were converted to finite element (FE) models by converting the voxels (Fig. 3B).

#### *Material Properties*

Osseous tissues of the vertebrae and cartilaginous endplates in this study were modeled as isotropic homogeneous linearly-elastic materials[12]. The texture parameter of each ligament was defined as nonlinear, as shown in Table 1. Intervertebral disc and intercostal ligaments were the only differing material properties.

#### *Boundary and Loading Conditions*

In the whole model, each disc was tied between its adjacent end plates, and each two contiguous superior and inferior

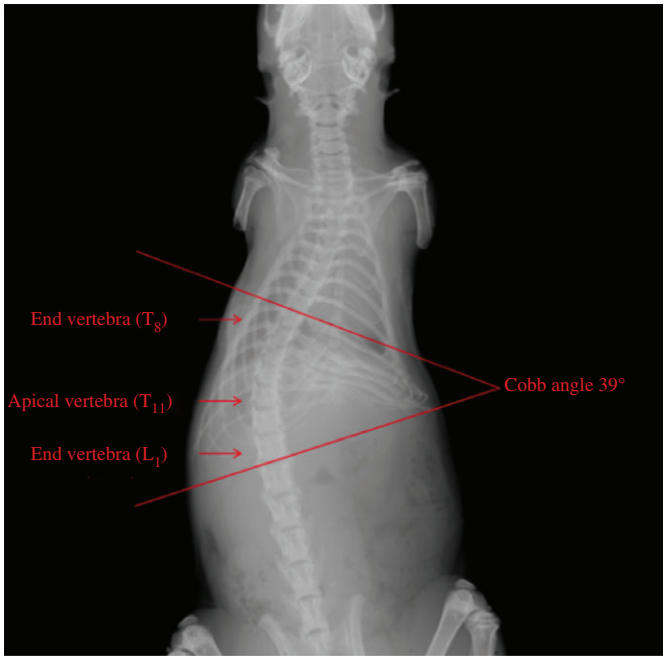


**Fig. 2** X-ray shows the dead rat scoliosis model (AP), and Cobb angle was 39.00°, and the apical vertebra of rats was $T_{11}$.

facets were set to sliding contact without friction. We assumed that gravity was the cause of axial loading. Axial loading of 2.4 N (calculated by measuring the dead rats) was applied to simulate the spine under gravitational force. The 3-D model was validated according to geometric validation. In this study, the FE model was first tested with pure unconstrained linear moments from 0 to 4 N under loading conditions of flexion, extension, and lateral bending (Fig. 4). We changed the size of force to ensure that the FE model of the spine was contrasted to the rat's X-ray plate to validate the model's geometric similarity according to their coincidence. The indexes of testing included coronal Cobb angle. Finally, resultant force (2.6 N) was given on $T_8$ on the left side to simulate asymmetric tension in the vertical direction.

Convex and concave sides of the apical vertebra were constructed using the ANSYS 14.5 FE package (ANSYS, Canonsburg, PA, USA). The FE model was used to compute the compressive stress distribution on the convex and concave sides. In this coordinate system, the X axis was pointing upward, the Y axis was oriented from right to left, and the Z axis was oriented anteriorly. In applying this method, the original geometries of the spine provided the biomechanical basis for asymmetric tension.

**TABLE 1 The module of model components in the finite element**

| Model component | Modulus (MPa) | Poisson's ratio |
|---|---|---|
| Vertebral body | 1000 | 0.3 |
| Rib | 1000 | 0.3 |
| Intervertebral disc | 3.5–14.9 | 0.3 |
| Intercostal ligaments | 1.5–6.5 | 0.3 |

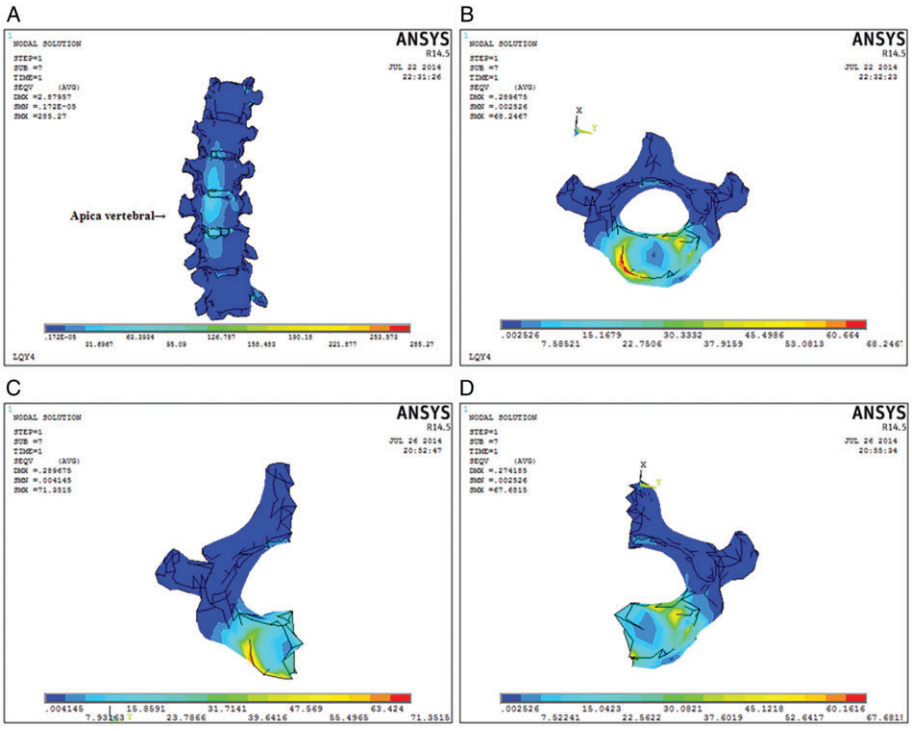


**Fig. 3** The reconstruction images of the spine ($T_8$–$L_1$). (A) Each scoliosis vertebra was divided into convex and concave sides by midcourt line. 3-D finite element (FE) model of the apical vertebra (B) shows typical difference in forces on the convex and concave sides. In resultant stress there was a difference between convex (C) and concave (D) sides (6593.02 *vs* 5022.48), and the convex side was observed to increase (31.27%) in the vertical direction of the vertebral body.

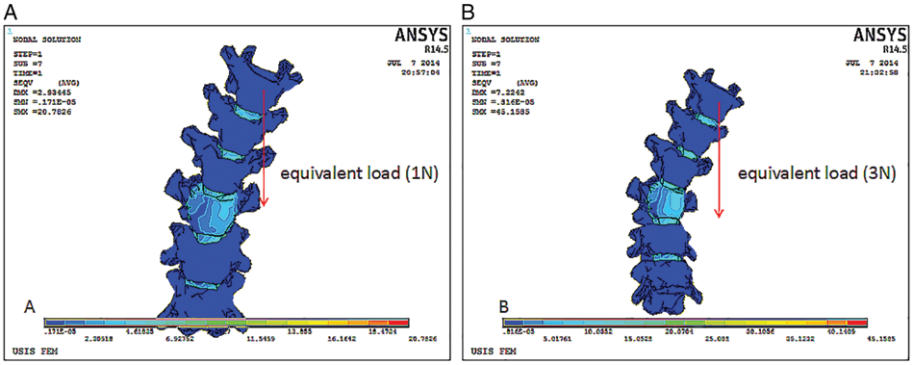


**Fig. 4** The finite element (FE) model was tested to simulate loading conditions. It shows reconstruction images of the spine under equivalent load 1 N (A) and 3 N (B). The force was given on $T_8$ in the vertical direction to simulate asymmetric tension.

### *Western Blot*

Vepiphyseal cartilage plates of four rats were harvested from the convex and concave sides. The protein samples were divided into two groups (convex group and concave group). Samples were carefully separated under a microscope. After washing with sterile phosphate-buffered saline (PBS), the attached connective tissue and muscle were removed. Then samples were stored in a saline-soaked gauze at −20°C until analysis[13]. Protein samples (−50 μg) were fractionated by SDS-PAGE (7.5%–10% polyacrylamide gels). Separated proteins were blot transferred onto a nitrocellulose membrane. After blocking with 0.1% Tween 20 and 5% nonfat dry milk in Tris-buffered saline at room temperature for 1 h, the membrane was incubated overnight at 4°C in the following primary antibodies: VEGF (R&D, USA) (1:200), Collagen Type X (Boster, CN) (1:400), collagen type Π (NeoMarkers, CA, USA) (1:400), Sox-9 (Santa Cruz, CA, USA) (1:500), aggrecan (Santa Cruz, CA, USA) (1:500), RUNX2 (Santa Cruz, CA, USA) (1:500) and β-actin (Santa Cruz, CA, USA) (1:1000) as an internal control. The membrane was incubated with horseradish peroxidase-conjugated secondary antibody (1:2000) for 1 h and detected using the Enhanced Chemiluminescence (ECL) Western blot System (Amersham Biosciences, Buckinghamshire, UK).

### *Micro-CT*

Four rats were assessed for bone quality based upon micro-CT images (μCT35, Scanco, MicroCT systems and Software, Brüttisellen, Zurich, Switzerland). Each scoliosis vertebra was divided into convex and concave sides by the midcourt line. The trabecular bone of cancellous bone was extracted from the vertebral body as a volume of interest (VOI) by mapping along the margin between the cortical shell and trabeculae.

**TABLE 2 Stress results of the apical vertebral in all directions (MPa)**

| Seqv value | Convex | Concave | Total |
|---|---|---|---|
| X axis | −170.14 | 361.99 | 191.88 |
| Y axis | −373.18 | 605.55 | 232.58 |
| Z axis | −3832.32 | 3661.95 | −171.65 |
| Stress results | 6593.02 | 5022.48 | 11615.20 |

The convex and concave sides were calculated using the built-in software of the μCT scanner, generating the following data: the bone volume fraction (BV/TV, fraction of trabecular bone per total volume); trabecular number (Tb.N, number of trabeculation per mm); trabecular thickness (Tb.Th, trabecular thickness); trabecular separation (Tb.Sp, distance of each trabeculation); and structure model index (SMI, index referring to the plate-like or rod-like structure of trabeculation).

### *Statistical Analysis*

Statistical analysis was performed using the computer program SPSS (version 20, SPSS, Chicago, IL, USA), and values were expressed as mean ± standard deviation (SD). All data had been tested and verified to be of a normal distribution, and the paired samples *t*-test was used for statistical analysis. A significance level of 0.05 was adopted.

## Results

### *Cobb Angles of Scoliosis Models*

The Cobb angle was measured by Image-Pro Plus 6.0 (version 6, Media Cybernetics, USA) (Fig. 1). X-rays showed that in the rat scoliosis models the Cobb angles ranged from 22° to 48° and always had kyphosis (1.88° ± 0.41°). The average and standard deviation of the Cobb angle in subjects with a main left thoracic deformity was 35.11° ± 7.62°.

### *Mechanical Stress*

Finite element analysis was carried out on the axial and transverse tension of the spine. The forces in all directions were computed using digital records and the direction and magnitude of the resultant stress are given in Table 2. Stresses of the convex side were −170.14, −373.18 and −3832.32 MPa (X, Y, Z, respectively). Relatively, the concave side showed stress of 361.99, 605.55 and, 3661.95 MPa, respectively. In the resultant stress there was a difference between convex and concave sides (6593.02 *vs* 5022.48, Fig. 3), and the convex side was observed to increase (31.27%) in the vertical direction of the vertebral body. Therefore, stress on the vertebral and epiphyseal plate is asymmetric.

### *Protein Expression of Vertebral Epiphyseal Plate*

Western blot results are shown in Fig. 3. The integrated option density (IOD) was computed by Image Pro Plus (version 6.0, Media Cybernetics, Beijing, China). The mean values of aggrecan, collagen type II, Sox 9, RunX2, VEGF, and collagen type X were 9510.42 ± 4363.33, 21 353.78 ± 1678.87, 17 462.43 ± 3281.85, 23 374.15 ± 2871.86, 23374.15 ± 4917.86, and 24.93 ± 3.52 on the convex group. The mean values of the other group were 1701.54 ± 844.40, 9548.80 ± 2062.11, 5617.48 ± 2467.14, 10245.89 ± 3677.83, 10245.89 ± 1471.85, and 7.17 ± 5.95 (Table 3). VEGF and aggrecan were typical markers of chondrogenic differentiation. Compared with the concave group, the convex group showed increases in aggrecan (458.93%), collagen type II (123.62%), Sox 9 (210.86%), RunX2 (128.13%), VEGF (129.15%), and collagen type X (247.70%). There were obvious differences between convex and concave sides in the levels of the chondrogenic markers ($P < 0.05$). Significant differences were noted in the contribution of collagen type II, collagen type X, and RunX2 between the convex and concave sides ($P < 0.01$, Fig. 5). These protein expression differences between the convex and concave sides tend to show asymmetry of endochondral ossification and, thus, might account for eventual IS development.

### *Micro-Architecture of Trabecular Bone*

Micro-CT scans of the apical vertebral revealed the micro-architecture of trabecular bone and returned numerical values so as to describe the bone quality of the apical vertebral (Fig. 6). The mean values of BV/TV, Tb.N, Tb.Sp, Tb.Th, and SMI for the convex and concave sides were 0.33 ± 0.02 versus 0.26 ± 0.02, 4.88 ± 0.19 versus 4.40 ± 0.17, 0.08 ± 0.01 versus 0.07 ± 0.00, 0.19 ± 0.01 versus 0.21 ± 0.01 and 0.36 ± 0.25 versus 0.83 ± 0.20 (Table 4). The asymmetry of micro-architecture of trabecular bone was observed in the convex and concave sides. Compared with the concave group, the convex group showed increases in the BV/TV (26.92%) and Tb.N (10.90%), as well as increases in the Tb.Sp (9.52%, $P < 0.05$). Asymmetry in IS is not only found in anatomy, but also found in micro-architecture and bone quality. Asymmetry of bone quality should be the result of asymmetric expression of protein on the epiphyseal cartilage plate.

## Discussion

Scoliosis is a complex 3-D structural deformity, involving lordotic and kyphosis lateral bending and rotation[14]. To study the asymmetrical growth of scoliosis, Roth first reported that scoliosis is caused by the spinal cord being relatively short or excessive growth of the spinal column[15,16]. Moreover, Porter considered that asymmetry of the spinal cord and vertebral growth may be the root cause of scoliosis[17,18]. Here we focus on asymmetric tension in scoliosis and its effects on the biomechanics and metabolism of the vertebral epiphyseal plate, principally exploring whether asymmetric tension could contribute to scoliosis development. In this paper, we first propose a concept of a vicious circle in scoliosis and provide an introduction on its pathogenic mechanism.

Animal models have played an important role in the study of scoliosis over the past 20 years[19–22]. In this study of complex scoliosis, bipedal rats fed in high cages were used as a model for the human spine. Asymmetric tension on the rat's thoracic vertebra contributed to spinal deformity. In the coronal plane, all samples' Cobb angles were greater than 10°. Asymmetric tension on bipedal rats creates a successful model of scoliosis. Knowledge of the microstructure changes contributing to scoliosis would be valuable.

The FE model can provide insight into the structure–functional relationships of bone and the forces involved[23]. Patient-specific FE models have been used to explore the effects of biomechanical factors on scoliosis[24]. Gravity and a pre-existent asymmetry curves in the spine were identified as scoliosis-promoting factors[25]. In our study, force analysis was evaluated using FE and showed that epiphyseal cartilage had asymmetric tension in the vertical direction and this tended to contribute to a vicious cycle of asymmetry asymmetric tension[26]. However, this alone cannot explain the root cause of scoliosis, for which the molecular players should be identified.

Longitudinal spine growth occurs through the epiphyseal cartilage plate[27]. Endochondral ossification depends upon a variety of cytokines that regulate stromal cell differentiation into cartilage cells, thereby regulating synthesis of type II collagen in cartilage cells[28]. Similarly, as one of the related Runt gene family members, RunX2 is involved in multiple cytokine interactions and adjustments to bone metabolism and bone formation. Zheng reports that in the cartilage generation process, Runx2 directly affects collagen

**TABLE 3 Integrated option density (IOD) of labeled proteins on the convex and concave sides (mean ± standard deviation)**

| Variables | Convex | Concave | *P*-value | *t*-value |
|---|---|---|---|---|
| Aggrecan | 9510.42 ± 4363.33 | 1701.54 ± 844.40 | 0.049 | 3.214 |
| Collagen type II | 21 353.78 ± 1678.87 | 9548.80 ± 2062.11 | 0.006 | 7.131 |
| Sox 9 | 17 462.43 ± 3281.85 | 5617.48 ± 2467.14 | 0.024 | 4.255 |
| RunX2 | 23 374.15 ± 2871.86 | 10 245.89 ± 3677.83 | 0.009 | 6.032 |
| VEGF | 23 374.15 ± 4917.86 | 10 245.89 ± 1471.85 | 0.048 | 3.241 |
| Collagen type X | 24.93 ± 3.52 | 7.17 ± 5.95 | 0.001 | 12.528 |

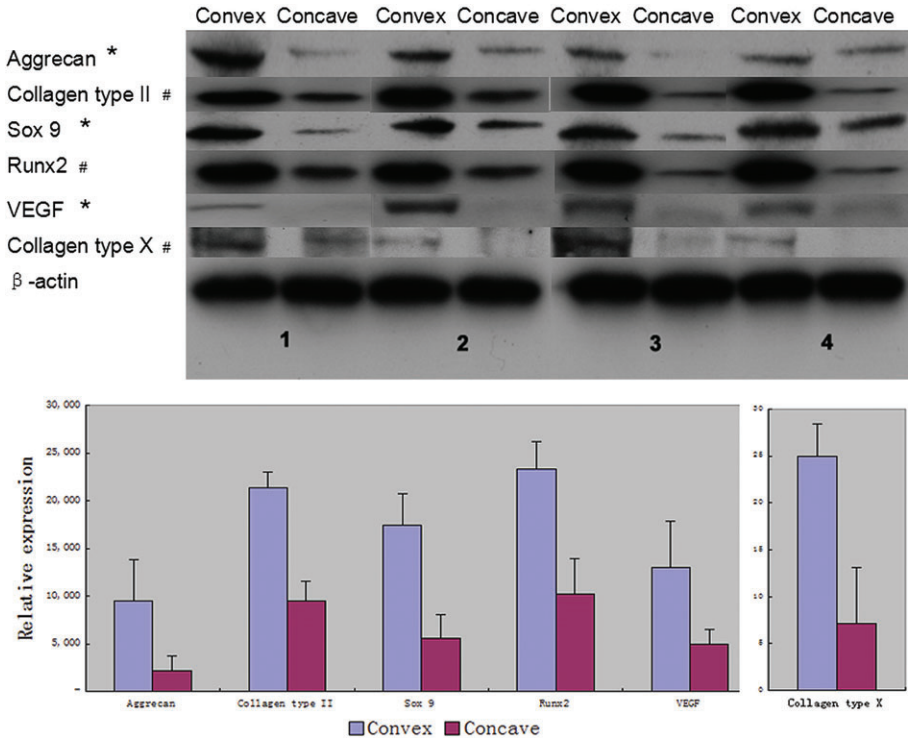


**Fig. 5** Expression of collagen type II, collagen type X, Sox 9, RunX2, VEGF, and aggrecan were assessed by western blotting. The different values from convex and concave sides were shown on the electrophorogram and column charts. All values are shown as mean ± SD. $^{*}P < 0.05$ and $^{\#}P < 0.01$.

type X genes and regulates the expression of collagen[29]. Type II collagen is the major structural protein of the epiphyseal plate cartilage, and as with type X collagen, cartilage proteoglycan glycans (Aggrcan) is evaluated together with the widely used chondrocyte proliferation. Reports have demonstrated that multiple VEGF are involved in the process of neovascularization[30]. The above proteins are key proteins related to growth of the epiphyseal cartilage plate, which have been reported in many studies. Synthesis and metabolism of protein are controlled by the upstream or downstream regulatory proteins. Despite the presence of interactions and adjustments, proteins on the epiphyseal cartilage present positive feedback in the growth stage. The biomechanics and metabolism of the vertebral–epiphyseal plate is easy to study.

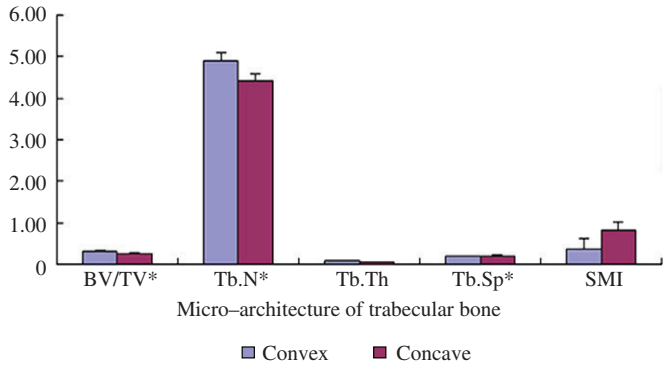


**Fig. 6** The column chart shows the micro-architecture of the apical vertebra trabecular bones. Numerical value was shown to describe the bone quality of the apical vertebra on convex and concave sides. All values are shown as mean ± SD. $^{*}P < 0.05$.

Bone quality describes bone micro-architecture and contributes to the level of bone turnover and bone microdamage. BV/TV is an index that reflects the amount of bone mass, whereas the Tb.Sp, Tb.Th, and SMI parameters better explain changes in bone microarchitecture[31]. Bone growth has been reported to be accompanied by increases in Tb.Th, BV/TV, and Tb.N, but decreases in Tb.Sp. In our study, there is a significant difference in the bone mass (BV/TV) between the convex group and the concave group, with the convex group having significantly higher BV/TV than the concave group, which is consistent with the expression of protein on epiphyseal cartilage plate. We propose that expression of protein on the epiphyseal cartilage plate contributed to the growth of bone density.

Before the onset of IS, there will have already been changes in the bone microstructure, conforming to Wolff's law. Through long-term and in-depth study of Wolff's law, it has been shown that the microstructure of bone dynamically adjusts and realigns itself in precise relation to changes in the loading direction[32,33]. This raises the possibility that a pathway exists, in which asymmetric tension affects molecular mechanisms to induce changes in vertebral epiphyseal plate microstructure, which subsequently act on the mechanical properties of the rat vertebral body. As children and adolescents grow and develop into adults, loading stresses bring about dynamic changes, which might exacerbate scoliosis.

**TABLE 4 Histomorphometry indices of the apical vertebral trabecular bones (mean ± standard deviation)**

| Variables | Convex | Concave | *P*-value | *t*-value |
|---|---|---|---|---|
| BV/TV (%) | 0.33 ± 0.02 | 0.26 ± 0.02 | 0.024 | 3.375 |
| Tb.N (1/mm) | 4.88 ± 0.19 | 4.40 ± 0.17 | 0.013 | 6.023 |
| Tb.Th (mm) | 0.08 ± 0.01 | 0.07 ± 0.00 | 0.130 | 1.960 |
| Tb.Sp (mm) | 0.19 ± 0.01 | 0.21 ± 0.01 | 0.027 | 3.286 |
| SMI | 0.36 ± 0.25 | 0.83 ± 0.20 | 0.062 | 0.1440 |

BV/TV, bone volume fraction (fraction of trabecular bone per total volume); Tb.N, trabecular number (number of trabeculation per mm); Tb.Th, trabecular thickness (trabecular thickness); Tb.Sp, trabecular separation (distance of each trabeculation); SMI, structure model index (index referring to the plate-like or rod-like structure of trabeculation).

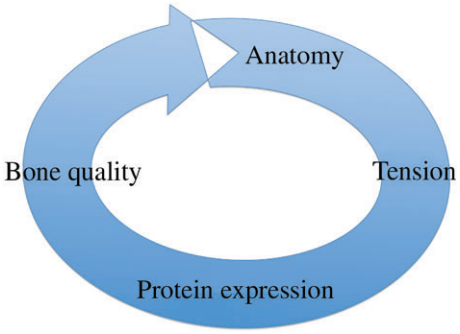


**Fig. 7** The cycle of asymmetry. Asymmetry of anatomy contributes to asymmetry of stress, then protein expression, then bone quality and eventually asymmetry of anatomy.

Scoliosis is a multifactorial disease. Previous studies might have focused on only one or two aspects. The lack of systematic assumptions could be problematic. We investigated the relationships among stress, protein expression, bone quality, and asymmetry of anatomy and suggested that there was an asymmetrical vicious circle in scoliosis, ultimately resulting in coronal decompensation (Fig. 7). This assumption can be explained as follows. First, we found that asymmetry of anatomy contributed to asymmetry of stress by building a scoliosis rat model and finite element analysis. Second, protein expression and bone quality on the convex and concave sides suggested that there was an asymmetry on micro-architecture of scoliosis, which also proved Wolff's theories. Third, eventually, asymmetry of protein expression and bone quality aggravated the deterioration of scoliosis. In addition, in the current research, most causes could be explained by this assumption. Genetic factors are always thought of as a possible contributor, as they may cause the asymmetry of protein expression leading to scoliosis. Because external fixation is used as a treatment for scoliosis, it is easy to explain that reducing the asymmetry of stress is the effective way to block the loop and, finally, to slow the progression of the disease.

This study has several limitations. First, the sample size is small: only 8 rats underwent this modeling and the overall result was good. Second, we did not present a control group without any rib tethering, which has indicated the effect of the regiment on the spine. The use of such a group will similarly enhance the bone histomorphometry and gene-based analysis. Third, modeling is confined to thoracic scoliosis, and the analysis of lumbar scoliosis might differ considerably from the results reported here. Tethering between ilium and ribs should greatly solve the problem. Our method is easier to operate and can be a supplement in cases for prospective studies of scoliosis. Fourth, while scoliosis is involved in whole spine changes at the mechanics and molecular level, in the present study only apical vertebra underwent experimental analysis and comparison between the convex and concave sides. Stress analysis of the whole spine would be expected to show compensatory bending in the lumbar spine. Microstructure and stress at each vertebral scoliosis do not mean the same thing. However, this method requires a large amount of work and strict control of models' individual differences. At this stage, analysis of apical vertebra in our study was effective and feasible and could be an option for these spine surgeons.

In conclusion, asymmetrical loading might be a cause of scoliosis, because genetic and neurohormonal factors have been identified as related etiological factors. Above all, the discovery of the vicious circle in scoliosis may lead to a more accurate description of the biomechanical behavior of the spine, which is crucial for the planning of surgical scoliotic correction.

## Acknowledgment

We thank Dr Yingjian Gao for his assistance with the animal surgery.

## References

**1.** Kane WJ. Scoliosis prevalence: a call for a statement of terms. Clin Orthop Relat Res, 1977, 126: 43–46.

**2.** Smit TH. The use of a quadruped as an in vivo model for the study of the spine-biomechanical considerations. Eur Spine J, 2002, 11: 137–144.

**3.** Fagan AB, Kennaway DJ, Oakley AP. Pinealectomy in the chicken: a good model of scoliosis?. Eur Spine J, 2009, 18: 1154–1159.
**4.** Braun JT, Ogilvie JW, Akyuz E, Brodke DS, Bachus KN. Creation of an experimental idiopathic-type scoliosis in an immature goat model using a flexible posterior asymmetric tether. Spine (Phila Pa 1976), 2006, 31: 1410–1414.
**5.** Zheng X, Sun X, Qiu Y, *et al*. A porcine early-onset scoliosis model created using a posterior mini-invasive method: a pilot study. J Spinal Disord Tech, 2014, 27: E294–E300.
**6.** Speer DP. Collagenous architecture of the growth plate and perichondrial ossification groove. J Bone Joint Surg Am, 1982, 64: 399–407.
**7.** Kouwenhoven JW, Vincken KL, Bartels LW, Castelein RM. Analysis of preexistent vertebral rotation in the normal spine. Spine (Phila Pa 1976), 2006, 31: 1467–1472.
**8.** Kim H, Lee CK, Yeom JS, *et al*. Asymmetry of the cross-sectional area of paravertebral and psoas muscle in patients with degenerative scoliosis. Eur Spine J, 2013, 22: 1332–1338.
**9.** Duart Clemente J, Llombart Blanco R, Beguiristain Gurpide JL. Morphological changes in scoliosis during growth. Study in the human spine. Rev Esp Cir Ortop Traumatol, 2012, 56: 432–438.
**10.** Frost HM. Wolff's Law and bone's structural adaptations to mechanical usage: an overview for clinicians. Angle Orthod, 1994, 64: 175–188.
**11.** Zhong ZM, Li T, Xu ZX, *et al*. Effect of melatonin on the proliferation and differentiation of chondrocytes from rat vertebral body growth plate in vitro. Int J Med Sci, 2013, 10: 1392–1398.
**12.** Kiapour A, Ambati D, Hoy RW, Goel VK. Effect of graded facetectomy on biomechanics of Dynesys dynamic stabilization system. Spine (Phila Pa 1976), 2012, 37: E581–E589.
**13.** Escalada F, Marco E, Duarte E, *et al*. Growth and curve stabilization in girls with adolescent idiopathic scoliosis. Spine (Phila Pa 1976), 2005, 30: 411–417.
**14.** Weinstein SL, Dolan LA, Cheng JC, Danielsson A, Morcuende JA. Adolescent idiopathic scoliosis. Lancet, 2008, 371: 1527–1537.
**15.** Roth M. Idiopathic scoliosis caused by a short spinal cord. Acta Radiol Diagn (Stockh), 1968, 7: 257–271.
**16.** Roth M. Idiopathic scoliosis from the point of view of the neuroradiologist. Neuroradiology, 1981, 21: 133–138.
**17.** Porter RW. The pathogenesis of idiopathic scoliosis: uncoupled neuro-osseous growth?. Eur Spine J, 2001, 10: 473–481.
**18.** Porter RW. Idiopathic scoliosis: the relation between the vertebral canal and the vertebral bodies. Spine (Phila Pa 1976), 2000, 25: 1360–1366.
**19.** Machida M, Dubousset J, Imamura Y, Iwaya T, Yamada T, Kimura J. An experimental study in chickens for the pathogenesis of idiopathic scoliosis. Spine (Phila Pa 1976), 1993, 18: 1609–1615.
**20.** Machida M, Saito M, Dubousset J, Yamada T, Kimura J, Shibasaki K. Pathological mechanism of idiopathic scoliosis: experimental scoliosis in pinealectomized rats. Eur Spine J, 2005, 14: 843–848.
**21.** Cheung KM, Wang T, Poon AM, Carl A, *et al*. The effect of pinealectomy on scoliosis development in young nonhuman primates. Spine (Phila Pa 1976), 2005, 30: 2009–2013.
**22.** Machida M, Dubousset J, Imamura Y, Miyashita Y, Yamada T, Kimura J. Melatonin: a possible role in pathogenesis of adolescent idiopathic scoliosis. Spine (Phila Pa 1976), 1996, 21: 1147–1152.
**23.** Rhee Y, Hur JH, Won YY. Assessment of bone quality using finite element analysis based upon micro-CT images. Clin Orthop Surg, 2009, 1: 40–47.
**24.** Pasha S, Aubin CE, Parent S, Labelle H, Mac-Thiong JM. Biomechanical loading of the sacrum in adolescent idiopathic scoliosis. Clin Biomech (Bristol, Avon), 2014, 29: 296–303.
**25.** Drevelle X, Dubousset J, Lafon Y, Ebermeyer E, Skalli W. Analysis of the mechanisms of idiopathic scoliosis progression using finite element simulation. Stud Health Technol Inform, 2008, 140: 85–89.
**26.** Fok J, Adeeb S, Carey J. FEM simulation of non-progressive growth from asymmetric loading and vicious cycle theory: scoliosis study proof of concept. Open Biomed Eng J, 2010, 4: 162–169.
**27.** Dickson RA, Deacon P. Spinal growth. J Bone Joint Surg Br, 1987, 69: 690–692.
**28.** Rabie AB, She TT, Hagg U. Functional appliance therapy accelerates and enhances condylar growth. Am J Orthod Dentofacial Orthop, 2003, 123: 40–48.
**29.** Zheng Q, Zhou G, Morello R, Chen Y, Garcia-Rojas X, Lee B. Type X collagen gene regulation by Runx2 contributes directly to its hypertrophic chondrocyte-specific expression in vivo. J Cell Biol, 2003, 162: 833–842.
**30.** Wakelee H, Kernstine K, Vokes E, *et al*. Cooperative group research efforts in lung cancer 2008: focus on advanced-stage non-small-cell lung cancer. Clin Lung Cancer, 2008, 9: 346–351.
**31.** Boyle C, Kim IY. Three-dimensional micro-level computational study of Wolff's law via trabecular bone remodeling in the human proximal femur using design space topology optimization. J Biomech, 2011, 44: 935–942.
**32.** Barak MM, Lieberman DE, Hublin JJ. Wolff in sheep's clothing: trabecular bone adaptation in response to changes in joint loading orientation. Bone, 2011, 49: 1141–1151.
**33.** Justice CM, Miller NH, Marosy B, Zhang J, Wilson AF. Familial idiopathic scoliosis: evidence of an X-linked susceptibility locus. Spine (Phila Pa 1976), 2003, 28: 589–594.